Testing Quintessence models with large-scale structure growth

K. Benabed, Francis Bernardeau

Testing quintessence models with large-scale structure growth

K. Benabed and F. Bernardeau
Service de Physique Théorique, CE de Saclay, F-91191 Gif-sur-Yvette Cedex, France
(Received 23 April 2001; published 18 September 2001)

We explore the possibility of putting constraints on quintessence models with large-scale structure observations. In particular, we compute the linear and second order growth rate of the fluctuations in different flavors of quintessence scenarios. We show that effective models of quintessence (e.g., with a constant equation of state) do not account for the results found in more realistic scenarios. The impact of these results on observational quantities such as the shape of the nonlinear power spectrum in weak lensing surveys or the skewness of the convergence field is investigated. It appears that the observational signature of quintessence models is specific and rather large. The effects clearly cannot be mistaken for a change of Ω_0.

DOI: 10.1103/PhysRevD.64.083501 PACS number(s): 98.80.Cq, 98.62.Sb, 98.65.Dx

I. INTRODUCTION

The recent evidence in favor of a nonzero cosmological constant [1–9] has led to the development of alternative scenarios to explain such a nonzero vacuum energy density [10]. In particular, models involving the so-called quintessence have attracted attention from the high-energy physics community [11–17]. Indeed, in such models the vacuum energy density is due to the potential and kinetic energy of a scalar field rolling down its potential. Various models have been proposed. The simplest implementation of such models, widely used in the literature, is to introduce an *effective* quintessence with a constant equation of state [11]. More elaborate theories provide potentials that exhibit a tracking solution regime as long as the energy density of the quintessence field is subdominant [13]. This behavior is generically encountered in the Ratra-Peebles [17] model in which the quintessence potential is a simple inverse power of the field. Other models inspired by high-energy physics have also been shown to exhibit this remarkable property [14–16].

The presence of a quintessence field changes the energy content of the universe and therefore alters its global expansion rate. It is then natural to try to detect the signature of a nonstandard vacuum equation of state through its impact upon the distance-luminosity function, which can be revealed by supernova type Ia (SNIa) observations [18–20]. It has been found, however, that the precision with which the vacuum equation of state can be measured depends crucially on whether priors are assumed on the other cosmological parameters, in particular on the matter content of the Universe. This calls for a reexamination of the theoretical foundations upon which precision methods for determination of the cosmic density are based.

The cosmic microwave background (CMB) anisotropy power spectrum has been recognized as a gold mine for the determination of cosmological parameters. It is actually a very valuable method for measuring the global curvature of the Universe [1] (through the value of the angular distance of the last scattering surface) but it suffers from an unavoidable parameter degeneracy [21,22] so that Ω_0 cannot be determined alone.

The impact of quintessence models on the properties of the CMB as well as on the primordial density contrast power spectrum has nonetheless been studied in different models: the *effective* quintessence (with the extra shortcoming that the possible fluctuations of the quintessence field were neglected) as well as some high-energy physics tracking *potentials* [14,23]. It has been found that at the redshift of recombination the dark energy fluid is subdominant and has only significant superhorizon fluctuations. Quintessence effects appear, therefore, only as a modest change of the Sachs-Wolfe plateau, an effect difficult to detect unambiguously because of the size of the cosmic variance.

It has been shown, however, that although the intrinsic properties of CMB anisotropies fail to provide an unambiguous test of quintessence, its existence can be shown by the amplitude of the density fluctuations on the last scattering surface compared to those at low redshift. This can be done, for instance, with the help of galaxy cluster counts [24,25] or with weak lensing measurements [26,27].

In all cases, however, direct constraints on Ω_0 that would help to disentangle models rely on analysis of the local universe properties. The matter content of galaxy clusters or their number density evolution [24,28] can provide useful constraints. Unfortunately these methods depend on nontrivial modeling of cluster properties such as x-ray luminosity or temperature-mass relations. It is therefore unlikely that they can provide accurate constraints on Ω_0 with a well controlled level of systematics.

New methods, based on weak lensing observations, are now emerging that are in principle free of elaborate physical modeling. The proposed means for constraining Ω_0 are based on the rate at which nonlinear effects start to play a role in the cosmic density field. Fundamentally, two ideas have been followed. One is based on the nonlinear evolution of the shape of the power spectrum [29] and preliminary results have already been reported in this case [27]. It relies on some specific class of models, namely, some flavor of cold dark matter (CDM) model (the shape of the nonlinear power spectrum obviously depends on what is assumed for the linear one). The other method, proposed in [30], is more demanding on the observation side but is based on the sole assumption that the initial conditions were Gaussian. It relies on the direct detection of non-Gaussian properties of the density field. In particular, it has been shown that the large-scale convergence skewness can be used to measure Ω_0. Exact

results obtained via second order perturbation theory have been obtained for models with or without a cosmological constant. It is then crucial to know whether these results would be affected in the case of quintessential dark energy.

The aim of this paper is therefore to examine the growth of structure in both the linear and the nonlinear regimes. To illustrate our results and their robustness we consider various realistic models of quintessence. So far the evolution of large-scale structure has been studied only with effective quintessence [11,31,32] and we will see that it does not provide a realistic account of what is happening in explicit models of quintessence.

This paper is divided as follows. In Sec. II we describe the models we use and in particular the evolution of the vacuum equation of state they imply. In Sec. III the results for the linear and second order growth rates are presented. Implications of these results are discussed in Sec. IV for the nonlinear power spectrum.

II. THE QUINTESSENCE MODELS

We postulate that the content of the universe includes a scalar field Q of potential V. This scalar field is responsible for the dark energy we observe today and is usually described as a cosmological constant. Its motion equation is given by the Klein-Gordon equation

$$\ddot{Q}+3H\,\dot{Q}=-\frac{\partial V}{\partial Q} \tag{1}$$

and it contributes to the energy and pressure terms with

$$\rho_Q=V(Q)+\frac{1}{2}\dot{Q}^2,$$

$$p_Q=-V(Q)+\frac{1}{2}\dot{Q}^2. \tag{2}$$

The equation of state of the dark energy

$$p_Q=\omega_Q\,\rho_Q \tag{3}$$

is *a priori* no longer characterized by a constant $\omega_Q=-1$ parameter. It can vary from $\omega_Q=-1$ when the dynamics of the field is dominated by its potential, to $\omega_Q=1$, when the kinetic energy dominates. In all the models we will consider, the parameters will be chosen so that $\Omega_0=0.3$ and $\Omega_Q=0.7$ today, unless otherwise mentioned.

In the following we focus our analysis on two models with tracking solutions that provide explicit time dependency of the equation of state, the Ratra-Peebles model [17] and the model developed by Brax and Martin in which the potential shape incorporates generic supergravity factors [15,16]. In this section we succinctly review the properties of the effective, Ratra-Peebles, and supergravity (SUGRA) quintessence models and compute the resulting equation of state of the Universe in these models.

A. Effective quintessence

Models of effective quintessence are the simplest implementations of a nontrivial vacuum equation of state. It is simply assumed that the equation of state parameter is fixed and represents an average value of a cosmic component following a complex evolution (whether or not it is a quintessence field). Considered as a simplified version of a quintessence model, this is a valid approach if, for some reason, the kinetic energy and the potential are almost constant and of the same order. This condition (which is *not* the slow-roll condition where the kinetic energy is much smaller than the potential) seems unlikely to be satisfied in a realistic framework. We will nonetheless compare realistic models with this approximation to show its impact on observed quantities.

B. Tracking quintessence

In a very wide class of quintessence models the field dynamics exhibits a tracking solution. It is such that the evolution of the dark energy, during radiation and matter domination, is completely determined by the potential shape regardless of the initial conditions.[1] In other words, the only tuning required to reproduce today's observations is the energy scale of the potential. Eventually, this scale will have to be explained by high-energy physics computations. While this task seems insuperable in the case of a pure cosmological constant, it might be within theoretical grasp for tracking quintessence [13,33].

The phenomenological properties of this class of models can be summarized through the time evolution of the cosmic equation of state. The detailed behavior of the field in the first stages of its evolution depends on the initial conditions. If initially ρ_Q represents a fair fraction of the cosmic energy density, the field Q rolls quickly down its potential so that the quintessence energy density is purely kinetic. It is slowed by the expansion until it freezes at a value larger than the one corresponding to the tracking solution. The value of the field then remains constant—the quintessence energy density is purely potential—until it coincides with the attractor solution. Once on the attractor solution, the equation of state parameter of the quintessence field takes a value that depends only on the shape of the potential and on the equation of state of the dominant species of the universe (it therefore changes at equivalence). When the energy density of the field starts to dominate, the field follows an inflationary type slow-roll solution whose equation of state is approaching $\omega_Q=-1$. These behaviors are displayed on Fig. 1 for the potentials we adopted. The time at which the tracking solution is reached is completely arbitrary and has no effect on the quantities we consider in the following.

Our analysis will be done for two tracking models.

First is the Ratra-Peebles model [17] whose potential is

$$V_{\rm RP}(Q)=\frac{M^{4+\alpha}}{Q^{\alpha}} \tag{4}$$

[1]Over hundred orders of magnitude.

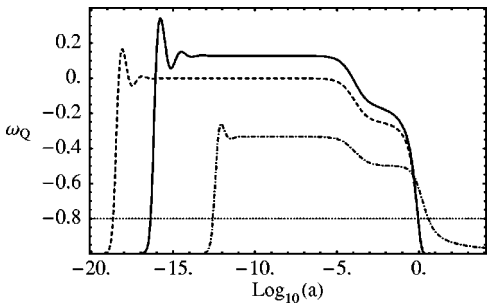

FIG. 1. The evolution of the vacuum equation of state as a function of the expansion parameter a for different cosmological models. The dotted line corresponds to a vacuum equation of state, $p=-0.8\rho$; the dot-dashed line to a Ratra-Peebles solution with $\alpha=2$; the dashed line to a SUGRA behavior with $\alpha=6$; and the solid line to a SUGRA model with $\alpha=11$. The amplitude of the quintessence potentials is such that $\Omega_{\mathrm{matter}}=0.3$ at $z=0$ in all cases.

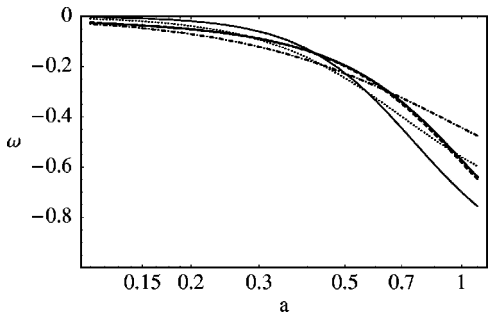

FIG. 2. The evolution of the global cosmic equation of state as a function of the expansion parameter a for different cosmological models for a redshift range $z=0$ to 10. Same convention as Fig. 1 with thin solid line corresponding to a pure cosmological constant such that $\Omega_\Lambda=0.7$ at $z=0$.

and which is the simplest model exhibiting a tracking solution. In particular, it is very hard, with this potential, to get an equation of state $\omega_Q<-0.7$ while keeping a reasonable energy normalization for M (from the high-energy physics point of view) if $\Omega_\Lambda=0.7$ today. Note that for such a potential the vacuum equation of state of the attractor solution is given by

$$\omega_Q=\frac{-2+\alpha\omega_B}{\alpha+2} \tag{5}$$

where ω_B is the equation of state parameter of the background fluid (1/3 for a radiation dominated universe, 0 for a matter dominated universe). In the following we will consider the case $\alpha=2$, which gives $\omega_Q\sim-0.6$ today, marginally consistent with the supernovae observations although it leads to an unrealistic low-energy scale for M.

Second, we consider the SUGRA model, proposed by Brax and Martin [16,15], whose potential is

$$V_{\mathrm{Sugra}}(Q)=\frac{M^{4+\alpha}}{Q^\alpha}\exp\left[4\pi\frac{Q^2}{M_{\mathrm{Planck}}^2}\right]. \tag{6}$$

The corrective factor is motivated by the fact that, in the Ratra-Peebles scenario, the field naturally reaches the Planck scale at low redshift. If the quintessence potential is to be derived from models beyond the standard model of particle physics that are expected to include supergravity properties, it is natural to expect supergravity corrections in the shape of the potential. The potential Brax and Martin proposed is actually an extension of the Ratra-Peebles potential, with a generic supergravity correction (the exponential term). This last model is of particular interest since its predictions are in good agreement, for a wide range of parameters, with the SNIa measurements. We studied here two examples of this potential, $\alpha=6$ and $\alpha=11$, which both lead to the equation of state $\omega_Q\sim-0.8$ at zero redshift. These choices of parameter lead to an energy scale M from 10^6 to 10^{11} GeV, which does not contradict our knowledge of high-energy physics.

The two models have the same tracking solution and the equation of state parameter on it is thus the same, given by Eq. (5). Differences between the two models arise when the field leaves the tracking solution. At this time, the field value is of the order of the Planck mass, and the SUGRA correction of the latter models starts to dominate. This SUGRA correction cures the problems encountered by the Ratra-Peebles potential by quickly slowing the field as it rolls down, thus providing a smaller equation of state parameter [16,15].

C. Solution of the equations with quintessence

The quintessence field contributes to the Friedman equations, and therefore to the evolution of the expansion rate of the universe,

$$\left(\frac{\dot a}{a}\right)^2=\frac{8\pi}{3M_{\mathrm{Planck}}}\rho_{\mathrm{tot}} \tag{7}$$

$$\frac{\ddot a}{a}=-\frac{4\pi}{3M_{\mathrm{Planck}}}(\rho_{\mathrm{tot}}+3p_{\mathrm{tot}}) \tag{8}$$

where ρ_{tot} is the total energy density of the Universe and p_{tot} its pressure, assuming we live in a zero curvature universe. It is convenient to define the parameter ω as the effective equation of state parameter of the ensemble of cosmic fluids,

$$p_{\mathrm{tot}}=\omega\,\rho_{\mathrm{tot}}. \tag{9}$$

This parameter is expected to vary from 1/3 in the radiation dominated era, $\omega=0$ in the matter dominated era, to $\omega\to-1$ when the vacuum energy dominates. The shape of this transition and its implication for the growth of structure are precisely what we investigate in this paper.

The evolutions of the equation of state of the universe are shown on Figs. 1 and 2. They show that the transition from a matter dominated universe $\omega=0$ to a vacuum dominated universe is much smoother in the case of quintessence models. In fact, the universe leaves the $\omega=0$ line much sooner in the tracking quintessence models than in the effective quintessence or the Λ models. It is then natural to expect significant effects on the angular distances or on the growth of

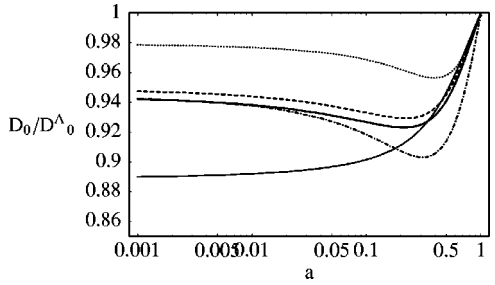

FIG. 3. Evolution of the comoving angular distance in the different scenarios compared to a pure cosmological constant from $z=1000$ to the local universe. Same conventions as in Figs. 1 and 2 are used for the line styles. The lower solid line corresponds to a pure cosmological constant model with $\Omega_0=0.4$.

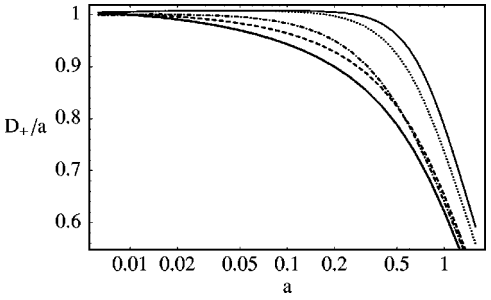

FIG. 4. The ratio D_+/a (normalized to unity at $z>100$) for the different scenarios. Today's growth rate is smaller by about 20% in tracking quintessence scenarios.

fluctuations. Moreover, the low-redshift behavior of the global cosmic equation of state is very different in the three quintessence models. This also should induce significant phenomenological differences between the Λ models and the quintessence models.

The implication of these behaviors for the angular distances is shown on Fig. 3. The differences seem not very noticeable at small redshift. However, they build up to be significant when the effect is integrated to the last scattering surface. The end values of the angular distances for the different tracking quintessence scenarios are very close to each other, although they correspond to different values of the equation of state today (see Fig. 2). Not surprisingly, quantities sensitive to the angular distance at high z, such as the position of the first acoustic peak, have been found to depend upon the vacuum equation of state [23]. One should also expect significant differences in the amplitude of the lens effect on the CMB anisotropies (as its depends on the angular distances between the observed objects and the lenses). We note however that a Λ model with a lower value of Ω_0 can reproduce fairly well the low-redshift behavior of the angular distances in our quintessence models.

III. THE GROWTH OF STRUCTURE

A. The linear growth rate

In the previous section we observed that, since the evolution of the universe with a quintessence component is smoother than with a pure cosmological constant, the departure from an Einstein–de Sitter (EdS) universe occurs later in the former case. This effect has been described before [32,11,12], although only in the context of effective quintessence, but it is clearly amplified here because the energy fraction of the quintessence field can be much larger at high redshift in cases of realistic quintessence models.

In this section we investigate the impact of these effects upon the evolution of large-scale structure. We consider the large-scale structure history only after recombination, a time at which the dark matter fluctuations dominate. After recombination and at subhorizon scales the quintessence field perturbations correspond to decaying modes and can therefore be ignored. Within these assumptions the growth rate of the density contrast at linear order is driven by the equation [34]

$$\ddot{D}_1(t)+2H\dot{D}_1(t)-\frac{3}{2}H^2\,\Omega(t)\,D_1(t)=0, \qquad (10)$$

where $\Omega(t)$ corresponds to the fraction of energy in the matter component. The growth rate is independent of the wavelength of the fluctuations as long as we consider fluctuation at subhorizon scale and if we neglect the pressure effects. The time evolution of D_1 provides the amplitude of the density fluctuations. Figure 4 gives the growth rate, for different models, as a function of redshift compared to the growth rate in the EdS case.[2] In models with a pure cosmological constant, the growth factor remains very close to the EdS solution for a long period, and then changes abruptly between redshift 2 and 3. In quintessence models the solutions follow the same scheme, yet with a smoother slope change. However, for the same normalization at $z>100$, when the universe is very close to an Einstein–de Sitter model, today's growth rates are quite different. The quintessence scenarios with a tracking field exhibit a smaller growth today (of order 20–30 % percent less). To say it in other words, for the same σ_8, the quintessence models demand larger density fluctuations at early times. This effect should lead to a difference between CMB normalizations and low-redshift normalizations.

The origin of this difference is clear. It is due to the fact that the energy fraction in the quintessence field remains significant for a much longer time. In this respect the effective quintessence solution is very similar to the Λ scenario, whereas realistic models of quintessence lead to linear growth rates that depart from the EdS case at redshift as large as 30. Clearly, models of effective quintessence that can match the SNIa observations do not provide a good account of the linear growth rates found in realistic models of quintessence.

B. Second order growth rate

As mentioned in the Introduction, for Gaussian initial conditions the second order growth rate determines the rate

[2]Whose solution is well known, $D_1(t)=a(t)$.

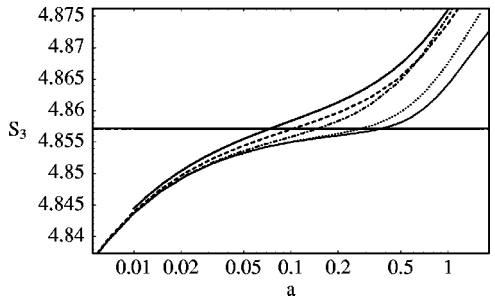

FIG. 5. The skewness for the different scenarios. The horizontal straight line gives the skewness in EdS models. The variations in the quintessence models are very small.

at which non-Gaussian properties emerge in the matter density field. In a perturbation theory approach it is indeed this quantity that determines the value of the large-scale skewness. Furthermore, it turns out that weak lensing surveys can be used as a test ground for this effect and provide a robust constraint on Ω_0 through the value of convergence skewness [35,30]. We examine here to what extent this approach remains valid in a quintessence cosmology.

Such perturbation theory calculations are based on the computation of higher order terms in a perturbative approach. More precisely the reduced skewness defined as

$$S_3 = \frac{\langle \delta^3 \rangle}{\langle \delta^2 \rangle^2} \tag{11}$$

can be related to the second order growth rate [36] and more specifically to the second order growth rate in spherical collapse dynamics [37,38]. In this case it is simple to expand the local density contrast to second order with respect to the initial density fluctuations,

$$\delta_{\rm sc}(t) = D_1(t)\,\delta_i + \frac{D_2(t)}{2}\,\delta_i^2 + \cdots, \tag{12}$$

with a time dependent coefficient that can be explicitly calculated for any cosmological model. The function $D_2(t)$ is the growing mode of the equation

$$\ddot{D}_2(t) + 2H\dot{D}_2(t) - \frac{3}{2}H^2\,\Omega(t)\,D_2(t) = 3H^2\,\Omega(t)\,D_1^2(t) + \frac{8}{3}\dot{D}_1^2(t). \tag{13}$$

The 3D density skewness at large scale (and when smoothing effects are neglected) is then directly proportional to $D_2(t)$, and is given by

$$S_3 = 3\,\frac{D_2(t)}{D_1^2(t)}. \tag{14}$$

From Fig. 5 it is clear that the variations of skewness with the cosmological models are very small (below the percent level) and are likely to remain undetectable. This means that the second order growth rate does not introduce further dependence on the vacuum equation of state. This result actually extends a property already known for the dependence of S_3 on Ω_0 for open universes [36], flat universes with a cosmological constant [38], or in some flavors of nonstandard vacuum equation of state [39].

TABLE I. Value of the skewness, Eq. (15), of the local convergence in weak lensing surveys for sources at redshifts 1 or 2 and for a power law index $n=-1.5$.

Skewness	$z_s=1$	$z_s=2$
Λ model ($\Omega_0=0.3$)	76	26
Λ model ($\Omega_0=0.25$)	85	28
$w_Q=-0.8$	83	28
Ratra-Peebles, $\alpha=2$	91	32
SUGRA, $\alpha=6$	85	30
SUGRA, $\alpha=11$	86	30

The skewness of the convergence is thus expected to be left unchanged, except through the dependence of the angular distances and the linear growth rate of the fluctuations. We recall here the formal expression for the convergence skewness in perturbation theory for a power law spectrum (of index n) [30]. For a flat universe, it is given by

$$s_3 = \frac{\displaystyle\int_0^{\mathcal{D}_s} d\mathcal{D}\, w^3(\mathcal{D})\, D_1^4(\mathcal{D})\, \mathcal{D}^{-2(n+2)} \left[S_3^{2D} - \frac{3}{2}(n+2) \right]}{\left[\displaystyle\int_0^{\mathcal{D}_s} d\mathcal{D}\, w^2(\mathcal{D})\, D_1^2(\mathcal{D})\, \mathcal{D}^{-(n+2)} \right]^2} \tag{15}$$

with an efficiency function $w(\mathcal{D})$ given by

$$w(\mathcal{D}) = \frac{3}{2}\,\Omega_0\,\frac{\mathcal{D}(\mathcal{D}_s - \mathcal{D})}{\mathcal{D}_s\, a} \tag{16}$$

where $\mathcal{D}_s$ is the comoving distance to the sources and s_3 is the skewness parameter for the 2D dynamics. The latter can be related to the 3D one, since it implies only a different combination of the terms appearing for the 3D case [38,30]. This finally gives

$$s_3 = \frac{3}{2} + \frac{9}{4}\,\frac{D_2}{D_1^2}, \tag{17}$$

which amounts to 36/7 for an Einstein–de Sitter case.

In Table I we present the expected skewness for the different models we have considered for sources at redshifts 1 or 2. The results show that the projection effects on the value of the skewness can be quite large. They increase the value of the skewness so that quintessence models with $\Omega_0=0.3$ mimic what one expects for a $\Omega_0=0.25$ model with a pure cosmological constant.

It is to be noted that angular diameter distances, in a quintessence scenario, rather resemble a Λ model with a *larger* value of Ω_0 (see Fig. 3). From those two joint observations it should then be possible to test the quintessence model hypothesis. However, results should be extended to the inter-

mediate and nonlinear regime where most of the data are going to be, although we expect the qualitative results found here to remain valid.

IV. NONLINEAR MATTER POWER SPECTRUM IN QUINTESSENCE MODELS

A. The shape of the nonlinear power spectrum

We complete these investigations with the nonlinear evolution of the matter density contrast power spectrum. Assuming a stable clustering ansatz and the Hamilton *et al.* mapping [40], we compare the power spectrum in quintessence and cosmological constant models in the deeply nonlinear regime.

The linear matter power spectrum in quintessence scenarios has been studied before [41,14,42,23]. For modes inside the horizons, models with a pure cosmological constant or with a quintessence field show very little difference in the shape of the linear transfer function. Limiting our study to those modes, we can reliably approximate the linear quintessence power spectrum by a standard cold dark matter model with a cosmological constant (ΛCDM) one.

However, there is no reason for the nonlinear evolution of these models to lead to the same power spectrum. Indeed, we showed in Sec. III A that generically the large-scale structure grows more slowly in quintessence scenarios. Hence, for the same amount of structure today, the density contrast had to be bigger in the quintessence scenario at early time. This implies that modes that are in the nonlinear regime now have reached this regime sooner in quintessence scenarios.

Following the idea of Hamilton *et al.* [40], later extended by Peacock and Dodds [43,44], we postulate that one can describe the effects of nonlinear evolution through a universal function $f_{\rm nl}$ that maps the linear power spectrum onto the nonlinear one:

$$\Delta^2_{\rm nl}(k_{\rm nl}) = f_{\rm nl}(\Delta^2(k)),$$
$$k = [1+\Delta^2_{\rm nl}(k_{\rm nl})]^{-1/3} k_{\rm nl}, \tag{18}$$
$$\Delta^2(k) = 4\pi k^3 P(k).$$

Enforcing stable clustering, Peacock and Dodds showed that this function must follow an asymptotic behavior at large x such that $f_{\rm nl}(x) \propto g(\Omega)^{-3} x^{3/2}$—where $g(\Omega) = D_1(a)/a$ is the ratio of the linear growth factor to the EdS growth factor described in Sec. III A—and proposed analytical forms for $f_{\rm nl}$ that depend on the cosmological parameters through $g(a)$ only and that are calibrated on various N-body simulations. We assume that their results hold for quintessence scenarios. In particular, we assume that the nonlinear regime always reaches a stable clustering regime. Moreover, and in the absence of quintessence N-body simulation for our particular scenarios, we also assume that the normalization factor in the asymptotic branch is independent of the cosmological scenario. These assumptions are not trivial and can probably be challenged (see, for instance, [32], where the behavior of the nonlinear power spectrum is investigated for effective quintessence models with a different perspective).

From the Hamilton *et al.* ansatz we expect very different behaviors for the small-scale nonlinear power spectrum when quintessence and nonquintessence models are compared. We previously obtained the result that about 20% to 30% discrepancy is expected, depending on the quintessence potential, between g^Q and D^Λ. The consequences of this *a priori* modest discrepancy are dramatic for the nonlinear power spectrum. For a mode that entered the non-linear region long before redshift z, we have

$$\frac{P^Q_{\rm nl}(k_{\rm nl},z)}{P^\Lambda_{\rm nl}(k_{\rm nl},z)} = \frac{\Delta^Q_{\rm nl}(k_{\rm nl},z)^2}{\Delta^\Lambda_{\rm nl}(k_{\rm nl},z)^2} \sim \frac{g^Q(z)^{-3}\,\Delta^Q(k_Q,z)^3}{g^\Lambda(z)^{-3}\,\Delta^\Lambda(k_\Lambda,z)^3} \tag{19}$$

where k_Q (k_Λ) is the linear mode in the quintessence (Λ) linear power spectrum giving rise to the $k_{\rm nl}$ mode in the nonlinear spectrum. Assuming, as stated before, that at the subhorizon scales we are interested in the linear power spectra of the models are identical, up to a normalization factor P_0, we write $P(k,z) = g^2(z) a^2 P_0 k^n$ with $n > -3$. For a mode in the nonlinear region we have

$$k \sim \left(\frac{k^2_{\rm nl}}{a^2 P_0}\right)^{1/(5+n)} \tag{20}$$

and Eq. (19) reduces to

$$\frac{P^Q_{\rm nl}(k_{\rm nl},z)}{P^\Lambda_{\rm nl}(k_{\rm nl},z)} \sim \frac{g^Q(z)^{-3}}{g^\Lambda(z)^{-3}} \left(\frac{g^Q(z)^2 a^2 P^Q_0 k_Q^{n+3}}{g^\Lambda(z)^2 a^2 P^\Lambda_0 k_\Lambda^{n+3}}\right)^{3/2}$$
$$\sim \left(\frac{P^Q_0}{P^\Lambda_0}\right)^{(3/2)[1-(n+3)/(n+5)]}. \tag{21}$$

We suppose here that the spectral index n is identical for both $P^Q(k_Q)$ and $P^\Lambda(k_\Lambda)$, which is a reasonable approximation. Finally, if we set both the spectra to fit the cluster normalization, the ratio P^Q_0/P^Λ_0 is simply the ratio of the growing modes at $z=0$ and we get

$$\frac{P^Q_{\rm nl}(k_{\rm nl},z)}{P^\Lambda_{\rm nl}(k_{\rm nl},z)} = \left(\frac{g^Q(z=0)}{g^\Lambda(z=0)}\right)^{-3\,[1-(n+3)/(n+5)]}. \tag{22}$$

Note that the exponent gets close to -3 when the spectral index goes to -3. Given the variation of g^Q the ratio given in Eq. (22) can be as large as 2.

The same ratio is easier to compute for modes in the linear regime,

$$\frac{P^Q(k,z)}{P^\Lambda(k,z)} = \left(\frac{g^Q(z)\,g^\Lambda(0)}{g^Q(0)\,g^\Lambda(z)}\right)^2. \tag{23}$$

These simple investigations show unambiguously and with a limited number of assumptions that the shape of the nonlinear power spectrum is very sensitive to the presence of a quintessence field. In order to have a full description of the power spectrum behavior, including the intermediate regime, we use the Peacock and Dodds prescription. This formula has been shown to be reasonably accurate for effective quin-

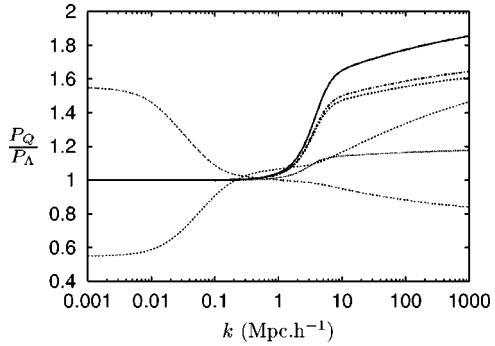

FIG. 6. The ratio P^Q_{3D}/P^Λ_{3D} at $z=0$. The solid and dashed lines are the SUGRA quintessence models for $\alpha=11$ and $\alpha=6$, the dot-dashed line is the Ratra-Peebles model, and the thin dotted line is the effective quintessence model for an a $\omega_Q=-0.8$. We also show here the results for a $\Omega_0=0.4$ flat ΛCDM model (thin dashed line) and an $\Omega_0=0.25$ flat ΛCDM model (thin double dashed line), which were discussed in previous sections.

tessence models in *N*-body simulation, at least at low redshift [32]. Anyway, we are more interested, in this paper, in the general trend rather than a completely accurate description of the transition between linear and nonlinear evolution. Figure 6 shows a comparison between quintessence models and a standard ΛCDM. The curves represent the ratios between a quintessence nonlinear P_{3D} at $z=0$ and the ΛCDM one assuming that the linear power spectra have the same normalization. As expected, the small-scale ratio tends toward the $(g^Q_+/g^\Lambda_+)^{-3}$ asymptote. The shape of the curve in this region is described by the $3[1-(n+3)/(n+5)]$ power calculated above. Since the effect is proportional to the growth ratio to the power 1/3, it is much smaller for effective quintessence where the discrepancy between its growth and the Λ model growth is smaller. We stress again therefore that the use of a constant equation of state cannot account for the amplitude of this effect as it is expected in realistic models.

Note that the transition between the linear and nonlinear regimes depends on the ansatz used for $f_{\rm nl}$. However, a very sharp transition, as encountered here, is not unnatural. It accounts for the different times a given mode enters the nonlinear regime in different models. If one follows a given mode throughout its evolution, it will first obey the linear growth and evolve as $a^2g^2(a)$. Then it enters the nonlinear regime and grows as a^3. The transition between these two regimes is very sharp. When models with a different growth factor are compared, this rapid transition translates into a sharp increase of the power spectrum ratio between the linear and nonlinear regimes.

Moreover, we note that this effect cannot be mistaken for a variation of Ω_0. The latter has a much more dramatic effect on the shape of the linear power spectrum through a change of the shape of the transfer function. In this case, not only is the linear growth rate changed but the position of the maximum of the linear power spectrum is also shifted.

In principle, large-scale galaxy surveys such as the 2dF or the SDSS should be able to put constraints on the amplitude and shape of the power spectrum. However, the possible effects of biasing mechanisms, which are extremely poorly understood in the transition regime between the linear and nonlinear regimes, prevent a robust and reliable test of these scenarios. In the next section we rather try to validate these properties in the context of a better defined observational procedure: the projected power spectrum in weak lensing surveys.

B. Projected power spectrum in weak lensing surveys

Weak lensing surveys can potentially provide us with precision maps of the projected density up to redshifts around 1 [45–48,26,49,27,50]. These measurements are expected to be free of observation biases once the redshift distribution of the sources is known.

Weak lensing surveys, through observation of the deformation of background galaxies, can give access to the convergence field. The latter can be written as the projection of the matter density along the line of sight [30],

$$\kappa(\vec{\alpha})=\int_0^{\mathcal{D}_s} d\mathcal{D}\, w(\mathcal{D})\,\delta(\vec{\alpha},z(\mathcal{D})), \tag{24}$$

where the $\mathcal{D}$ stands for the angular distance (and this formula is valid for a flat spatial curvature only). The geometrical kernel $w(\mathcal{D})$, defined in Eq. (16), accounts for the projection effects.

We expect that the ratio of the power spectra of the convergence field for models with a cosmological constant and models with a quintessence field will exhibit roughly the same properties as the ratio of the three-dimensional power spectra. However, the value of this ratio is expected to be affected by a corrective factor induced by the geometrical kernel which itself depends on the details of the cosmological model. In the following we present an evaluation of this rescaling factor along the line of reasoning of the previous subsection.

In the small-angle limit, we have

$$P_\kappa(\vec{\alpha})=\int_0^{\mathcal{D}_s} d\mathcal{D}\, w(\mathcal{D})^2 \int \frac{d^2k}{(2\pi)^2} P_{3D}(k,z(\mathcal{D}))e^{i\vec{k}\mathcal{D}\cdot\vec{\alpha}} \tag{25}$$

so that the convergence power spectrum is simply

$$P_\kappa(l)=\int_0^{\mathcal{D}_s}\frac{d\mathcal{D}}{\mathcal{D}^2} w(\mathcal{D})^2 P_{3D}(l/\mathcal{D},z(\mathcal{D})), \tag{26}$$

where a possible redshift evolution of the shape of the power spectrum is included. The kernel w is a bell shaped window that reaches its maximum at $z_{\rm eff}=z(\mathcal{D}_s/2)$. To evaluate roughly the rescaling factor we will approximate w^2 by a simple Dirac function $w^2(\mathcal{D})\sim w^2_{\rm eff}\,\delta(\mathcal{D}-\mathcal{D}_s/2)$ with $w_{\rm eff}=\int^{\mathcal{D}_s} d\mathcal{D}\, w(\mathcal{D})$ and $z_{\rm eff}\sim 0.4$ (it depends on the cosmology we are considering) for sources at redshift z_s. Now, the ratio of the convergence power spectrum is simply

$$\frac{P^Q_\kappa(l)}{P^\Lambda_\kappa(l)}\sim\left(\frac{w^Q_{\rm eff}/\mathcal{D}^Q_s}{w^\Lambda_{\rm eff}/\mathcal{D}^\Lambda_s}\right)^2\frac{P^Q_{3D}(2\,l/\mathcal{D}^Q_s,z^Q_{\rm eff})}{P^\Lambda_{3D}(2\,l/\mathcal{D}^\Lambda_s,z^\Lambda_{\rm eff})}. \tag{27}$$

TABLE II. Evaluation of the ratio $P_\kappa^Q/P_\kappa^\Lambda$ in the linear domain, from Eq. (29).

	$z=1$	$z=2$	$z=1000$
$\omega_Q=-0.8$	0.94	0.95	1.06
Ratra-Peebles $\alpha=2$	0.86	0.88	1.20
SUGRA $\alpha=6$	0.92	0.92	1.16
SUGRA $\alpha=11$	0.91	0.91	1.18

For a mode in the nonlinear region, a few percent error in the position of the mode is not significant, so that we can ignore the difference between D_Q and D_Λ in the last term of the equation. As a result,

$$\frac{P_\kappa^Q(l_{\rm nl})}{P_\kappa^\Lambda(l_{\rm nl})}\sim\left(\frac{w_{\rm eff}^Q/\mathcal{D}_s^Q}{w_{\rm eff}^\Lambda/\mathcal{D}_s^\Lambda}\right)^2\left(\frac{a_{\rm eff}^Q}{a_{\rm eff}^\Lambda}\right)^3 \times\left(\frac{g^Q(z=0)}{g^\Lambda(z=0)}\right)^{-3\,[1-(n+3)/(n+5)]}, \quad (28)$$

which, compared to Eq. (22), contains an extra geometrical factor due to the projection effects. It evaluates to 0.8 to 0.9 depending on the model and position of the source plane. We expect therefore the conclusions reached in the previous section to survive in weak lensing observations.

Similarly, for a mode in the linear region, we have

$$\frac{P_\kappa^Q(l)}{P_\kappa^\Lambda(l)}\sim\left(\frac{w_{\rm eff}^Q/\mathcal{D}_s^Q}{w_{\rm eff}^\Lambda/\mathcal{D}_s^\Lambda}\right)^2\left(\frac{a_{\rm eff}^Q}{a_{\rm eff}^\Lambda}\right)^2\left(\frac{g^Q(z_{\rm eff}^Q)}{g^Q(0)}\frac{g^\Lambda(0)}{g^\Lambda(z_{\rm eff}^\Lambda)}\right)^2. \quad (29)$$

Table II gives the value of the expected ratio in the linear region. It is about 0.9. This indicates that the normalization ratio for the linear 3D power spectrum and that for the projected weak lensing spectrum will differ by this amount.

These semianalytical results give a good account of the ratio $P_\kappa^Q/P_\kappa^\Lambda$ for all angular scales. At large scale, it is roughly flat; its value is given in Table II. Then, as we get closer to the transition between the linear and nonlinear regimes, the ratio exhibits a slight drop. Indeed, from Eq. (27) the ΛCDM model enters the nonlinear regime earlier, because of the difference between the $z_{\rm eff}$. Hence, one expects to have, for a few modes, a P_κ^Λ that rises more quickly than its quintessence counterpart. Then, when the quintessence power spectrum also hits the nonlinear regime, the ratio will exhibit a shape very similar to that of the three-dimensional power spectrum ratio, with the rescaling factor computed above.

In Fig. 7 we present the explicit computation of the nonlinear power spectra of the convergence field using the prescription of Peacock and Dodds to compute the redshift evolution of the 3D power spectrum. Unlike in Fig. 6, here the power spectra are not cluster normalized. In this case the power spectra are normalized so that the weak lensing amplitudes match at $10'$ scale when computed with the linear power spectrum and match the amplitude of the recent detections of weak lensing effects (e.g., $\sigma_8\approx 1$ for a ΛCDM model with $\Lambda=0.7$). Because of the projection effects given in Table II, this is not equivalent to the normalized linear 3D power spectrum. Projection effects also slightly change the shape of the projected linear power spectrum. The redshift of the sources is simply assumed to be unity here. The differences in the shape of the power spectra are clearly visible and should be already within observational constraints.

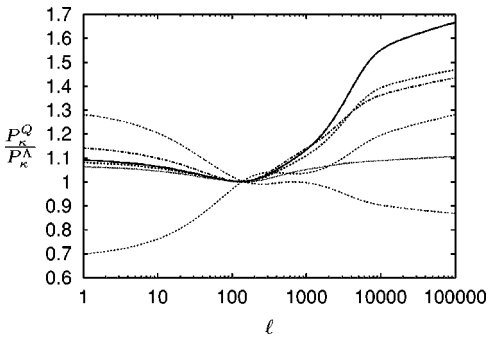

FIG. 7. Ratios $P_\kappa^Q(l)/P_\kappa^\Lambda(l)$ for a source plane at $z=1$. All models are normalized so that σ_κ are the same at $10'$ scale and correspond to an $\Omega_0=0.3$ flat ΛCDM model with $\sigma_8=1$. The observational window, in which measurements with an accuracy better than 10% are foreseeable, corresponds to l of 200 to 10 000 (minute to degree scale) where the most dramatic changes take place.

We also give the effects of a change of Ω_0, following the same prescription for the normalization. In this case, because we normalized to the *convergence* linear power spectrum, the change of Ω_0 also directly affects the normalization. Compared to 3D power spectra, it actually worsens the situation and make the distinction between quintessence models and such models striking.

The result of Fig. 7 gives us hope to strongly constrain the quintessence scenario using weak lensing surveys. The next generation weak lensing surveys will made available wide surveys where a precise determination of the lensing effect will be possible for a range of scales large enough to map the sharp rise predicted here. For example, measurements of the weak lensing effect amplitude at the 1° scale and the $1'$ scale with only a 10% precision appear sufficient to test the SUGRA quintessence hypothesis. It seems that the observational requirements are much more modest than for direct measurements of the angular distances through SNIa observations.

C. Weak lensing on cosmic microwave background

In passing we note that weak lensing effects on CMB maps could also be used to test the quintessence hypothesis. The amplitude of the effect is mainly given by the amplitude of the fluctuations of κ, σ_κ^2, along the line of sight [51,52]. In Table III we show the amplitude of the lens effect on the last scattering surface at two different angular resolutions. The amplitude is mainly sensitive to the linear change of the growth rate integrated over the line of sight. It would probably not be a crucial test for the nature of the vacuum energy but it is potentially an important test to pass once the general cosmological parameters are determined. If the coming generation of observations requires quintessence, observation of

TABLE III. Ratios between the amplitudes of the lens effects on the last scattering surface for different models and the standard ΛCDM model ($\Lambda = 0.7$) at two different angular resolutions.

σ_κ^2 at $z = 1000$	$5'$	$10'$
$\Omega = 0.25,\ \Lambda = 0.75$ model	1.23	1.29
$\Omega = 0.4,\ \Lambda = 0.6$ model	0.68	0.73
$\omega_Q = -0.8$	1.20	1.21
Ratra-Peebles $\alpha = 2$	1.49	1.54
SUGRA $\alpha = 6$	1.29	1.32
SUGRA $\alpha = 11$	1.33	1.36

an excess of power in the lens effect as suggested by these calculations will be an important consistency test.

V. CONCLUSION

In this paper we have examined the growth of structure in quintessence models in both the linear and the second order regimes and present their more striking implications for the statistical properties of the low-redshift large-scale structure of the universe. We paid particular attention to cases of realistic implementations of the quintessence field since they lead to scenarios where the energy fraction in the quintessence component can represent a significant fraction of the total energy density over a long period. We found that this effect is responsible for important differences in the behavior of the linear growth rate of the fluctuations: For the same values of Ω_0, realistic quintessence models lead to a linear growth rate that can be 20% or 30% lower than in models with a pure cosmological constant or with an effective quintessence component (where the vacuum has a constant equation of state which matches the angular distance constraints).

The consequences of this discrepancy have been explored at the level of the nonlinear power spectrum for which such differences are amplified. For power spectra with identical linear normalization (at $z = 0$), the variation of the amplitude of the nonlinear power spectrum can be as large as 2.

We have also computed the second order growth rate of the fluctuation. We found that, when expressed in terms of the square of the linear rate, it is not sensitive to the nature of the dark energy. This ratio is actually not significantly sensitive to any of the cosmological parameters. In this respect our result extends previously known properties.

Weak lensing surveys appear to be the natural playground for such effects. They combine effects on the angular distances and on the growth rate of the fluctuations. We show that the skewness of the convergence field, at large angular scale, is notably sensitive to the projection effects. It is to be noted, however, that a universe with a quintessence field does not resemble a universe with a cosmological constant and larger matter density (as is the case for the behavior of the angular distances) but rather one with a lower density parameter.

Moreover, the shape of the power spectrum of the convergence field, which can be identified with a projected 3D matter power spectrum, retains the properties found for the 3D nonlinear spectrum. It appears clear that CDM family models for a flat universe can be distinguished from one another: a variation of Ω_0 changes the shape of the linear power spectrum, whereas the introduction of a quintessence field changes the time at which modes become nonlinear.

The precision level of the current semianalytical predictions for the shape of the nonlinear spectrum does not permit us so far to make precise predictions from which the quintessence potential could be reconstructed. Moreover, the use of the prescription of Peacock and Dodds for models of quintessence with a tracking solution should probably be validated with specific numerical simulations.

The calculations have been done in two specific models of quintessence, the Ratra-Peebles model and the SUGRA model developed in [16]. We think, however, that our conclusions would survive for any model where the energy density in the quintessence component can be a significant fraction of the total energy up to recombination.

ACKNOWLEDGMENTS

The authors are very thankful to J. Martin, A. Riazuelo, Ph. Brax, and L. van Waerbeke for fruitful discussions.

[1] P. de Bernardis *et al.*, Nature (London) **404**, 955 (2000).
[2] A. E. Lange *et al.*, Phys. Rev. D **63**, 042001 (2001).
[3] P. M. Garnavich *et al.*, Astrophys. J. Lett. **493**, L53 (1998).
[4] S. Hanany *et al.*, Astrophys. J. Lett. **545**, L5 (2000).
[5] A. Balbi *et al.*, Astrophys. J. Lett. **545**, L1 (2000).
[6] S. Perlmutter *et al.*, Astrophys. J. **517**, 565 (1999).
[7] S. Perlmutter *et al.*, Nature (London) **391**, 51 (1998).
[8] A. G. Riess *et al.*, Astron. J. **116**, 1009 (1998).
[9] I. Waga and J. A. Frieman, Phys. Rev. D **62**, 043521 (2000).
[10] S. Weinberg, Rev. Mod. Phys. **61**, 1 (1989).
[11] I. Zlatev, L. Wang, and P. J. Steinhardt, Phys. Rev. Lett. **82**, 896 (1999).
[12] M. Tegmark, astro-ph/0101354.
[13] P. J. Steinhardt, L. Wang, and I. Zlatev, Phys. Rev. D **59**, 123504 (1999).
[14] P. G. Ferreira and M. Joyce, Phys. Rev. D **58**, 023503 (1998).
[15] Ph. Brax and J. Martin, Phys. Rev. D **61**, 103502 (2000).
[16] Ph. Brax and J. Martin, Phys. Lett. B **468**, 40 (1999).
[17] B. Ratra and P. J. E. Peebles, Phys. Rev. D **37**, 3406 (1988).
[18] T. D. Saini, S. Raychaudhury, V. Sahni, and A. A. Starobinsky, Phys. Rev. Lett. **85**, 1162 (2000).
[19] P. Astier, astro-ph/0008306.
[20] D. Huterer and M. S. Turner, astro-ph/0012510.
[21] M. Zaldarriaga, D. N. Spergel, and U. Seljak, Astrophys. J. **488**, 1 (1997).
[22] G. Efstathiou and J. R. Bond, Mon. Not. R. Astron. Soc. **304**, 75 (1999).
[23] Ph. Brax, J. Martin, and A. Riazuelo, Phys. Rev. D **62**, 103505 (2000).
[24] V. R. Eke, S. Cole, and C. S. Frenk, Mon. Not. R. Astron. Soc. **282**, 263 (1996).

[25] J. R. Bond *et al.*, astro-ph/0011379.
[26] R. Maoli *et al.*, astro-ph/0011251.
[27] L. van Waerbeke *et al.*, astro-ph/0101511.
[28] J. Oukbir and A. Blanchard, Astron. Astrophys. **317**, 1 (1997).
[29] B. Jain and U. Seljak, Astrophys. J. **484**, 560 (1997).
[30] F. Bernardeau, L. van Waerbeke, and Y. Mellier, Astron. Astrophys. **322**, 1 (1997).
[31] L. Hui, Astrophys. J. Lett. **519**, L9 (1999).
[32] C. Ma, R. R. Caldwell, P. Bode, and L. Wang, Astrophys. J. Lett. **521**, L1 (1999).
[33] P. Binetruy, Phys. Rev. D **60**, 063502 (1999).
[34] P. J. E. Peebles, *The Large-Scale Structure of the Universe* (Princeton University Press, Princeton, NJ, 1980).
[35] L. van Waerbeke, F. Bernardeau, and Y. Mellier, Astron. Astrophys. **342**, 15 (1999).
[36] F. R. Bouchet, R. Juszkiewicz, S. Colombi, and R. Pellat, Astrophys. J. Lett. **394**, L5 (1992).
[37] F. Bernardeau, Astrophys. J. **392**, 1 (1992).
[38] F. Bernardeau, Astrophys. J. **433**, 1 (1994).
[39] E. Gaztañaga, and J. A. Lobo, Astrophys. J. **548**, 47 (2001).
[40] A. J. S. Hamilton, A. Matthews, P. Kumar, and E. Lu, Astrophys. J. Lett. **374**, L1 (1991).
[41] J. C. Fabris and J. Martin, Phys. Rev. D **55**, 5205 (1997).
[42] R. R. Caldwell, R. Dave, and P. J. Steinhardt, Phys. Rev. Lett. **80**, 1582 (1998).
[43] J. A. Peacock and S. J. Dodds, Mon. Not. R. Astron. Soc. **280**, L19 (1996).
[44] J. A. Peacock and S. J. Dodds, Mon. Not. R. Astron. Soc. **267**, 1020 (1994).
[45] L. van Waerbeke *et al.*, Astron. Astrophys. **358**, 30 (2000).
[46] D. J. Bacon, A. R. Refregier, and R. S. Ellis, Mon. Not. R. Astron. Soc. **318**, 625 (2000).
[47] D. M. Wittman *et al.*, Nature (London) **405**, 143 (2000).
[48] N. Kaiser, G. Wilson, and G. Luppino, astro-ph/0003338.
[49] G. Wilson, N. Kaiser, and G. Luppino, astro-ph/0102396.
[50] J. Rhodes, A. Refregier, and E. J. Groth, astro-ph/101213.
[51] F. Bernardeau, Astron. Astrophys. **324**, 15 (1997).
[52] U. Seljak and M. Zaldarriaga, Phys. Rev. Lett. **82**, 2636 (1999).